J Mater Sci (2008) 43:6139–6143
DOI 10.1007/s10853-008-2936-z

Abnormal Hall–Petch behavior in nanocrystalline MgO ceramic

David Ehre · Rachman Chaim

Received: 10 April 2008 / Accepted: 6 August 2008 / Published online: 26 August 2008

Abstract Pure and dense nanocrystalline MgO with grain size ranging between 25 and 500 nm were prepared by hot-pressing. Vickers microhardness was found to increase with decrease in the grain size down to 130 nm, following the Hall–Petch relation. Further decrease in the grain size was followed by continuous decrease in microhardness. A composite model was used to describe the microhardness behavior in terms of plastic yield of the nanocrystalline grains accompanied by strain accommodation and nano-cracking at the grain boundaries (gb's). Good agreement between the experimental and the calculated values indicates that gb's may have significant effect on strengthening and ductility of nanocrystalline-MgO ceramics in the nanometer size range. Critical grain size exists below which limited plastic deformation within the grains and nano-cracking at gb's enhance the brittleness of the ceramic.

Introduction

Conventional MgO has excellent high temperature refractoriness and thus necessitates relatively high temperatures for powder consolidation and sintering. Fabrication of dense MgO ceramics often necessitates sintering temperatures above 1,600 °C. This was motivated fabrication of the ultrafine and nanocrystalline MgO (nc-MgO) powders using the hydroxide precursor prior to compaction [1–3]. Decrease in particle size of MgO powder was found to result in a nearly fully dense, transluscent bodies with sub-micron grain size [4]. Vast amount of research was dedicated to densification of MgO by hot-pressing [5–8]. Recently, transparent nc-MgO was fabricated using spark plasma sintering [9]. On the other hand, MgO is also characterized by a relatively low hardness and undergoes plastic deformation at elevated temperatures [10, 11].

In the last two decades several nanocrystalline metallic systems were reported to exhibit abnormal Hall–Petch behavior below a critical grain size [12–15]. Numerous models were also developed to explain the origin of this abnormal behavior [i.e., 16–21]. However, this effect was not studied in the ceramic systems mainly due to their brittle character as well as the difficulties in fabrication of fully dense nanocrystalline ceramics. Nevertheless, deformation of single crystal and polycrystalline MgO as model system has been studied extensively; its elastoplastic behavior resembles plastic behavior similar to the metallic systems [22–25]. In this respect, characterization of the room temperature plastic behavior of MgO and its grain size dependence in the nanometer range is interesting; it may have significant impact on fabrication processes of other ductile oxide systems (i.e., tin, lead, zinc, and indium oxides) with functional properties.

Experimental procedures

Commercial pure nc-MgO powder (Nanomaterials Res. Inc., USA) with specific surface area of 145 $m^2\ g^{-1}$ and calculated spherical diameter of 11 nm was used for hot-pressing. The hot-pressing conditions were described in detail elsewhere [8]. Dense disk-shape nc-MgO specimens were fabricated at different hot-pressing conditions. A series of specimens, exhibiting similar corrected relative densities (see below), with average grain size (diameter)

D. Ehre · R. Chaim (✉)
Department of Materials Engineering, Technion-Israel Institute of Technology, Haifa 32000, Israel
e-mail: rchaim@technion.ac.il

Table 1 Fabrication parameters and properties of hot-pressed nc-MgO specimens

No.	Temp (°C)-pressure (MPa)-duration (h)	Measured density (%)	Corrected density[a] (%)	Average grain size (nm)	Vickers microhardness (GPa)
1	790-150-2	93.6	97.0	27 ± 7	8.5 ± 0.9
2	790-100-1	94.0	96.0	50 ± 10	9.5 ± 1.7
3	790-100-2	94.0	96.0	130 ± 30	13.0 ± 1.5
4	790-100-4	95.5	96.0	280 ± 170	11.6 ± 0.9
5	900-50-1	97.0	97.0	450 ± 140	8.9 ± 1.7

[a] Using Eq. 1 in Ref. [26] and grain boundary thickness of 1 nm

between 27 and 450 nm (Table 1), were selected. The density of the specimens was measured by the Archimedes technique using the 2-propanol as the immersion liquid. The surfaces of these specimens were polished prior to the Vickers microhardness tests, using 0.25 μm diamond paste. The microhardness was determined using a 1-kg load in Vickers microhardness tester (Buehler Ltd.) while averaging over ten different test results from different locations at a given specimen. This load was the maximum load at which no cracks were observed around the indents; it was used to avoid the indentation size effects at low indentation loads. The average diagonal of the microhardness indents was about 40 μm. This diagonal size is higher by more than two orders of magnitude compared to the largest grain size tested, thus providing large number of the grains to be associated with the plastically deformed volume of the indent. The microhardness test duration was 10 s (indentation depth of ~3.2 μm) and the indent size was measured within 10 s from the load removal in order to avoid any effects of time-dependent plastic relaxations.

The microstructure was characterized using high-resolution scanning electron microscope (HRSEM, Leo Gemini 982 FEG) operated at 4 kV. No coating was applied to the SEM specimens. HRSEM images were used to determine the average grain size and its distribution via image analysis (Scion image-NIH). At least 200 grains were counted for a given specimen statistics. Selected specimens were also characterized using high-resolution transmission electron microscopy (HRTEM, Jeol-3010) operated at 300 kV.

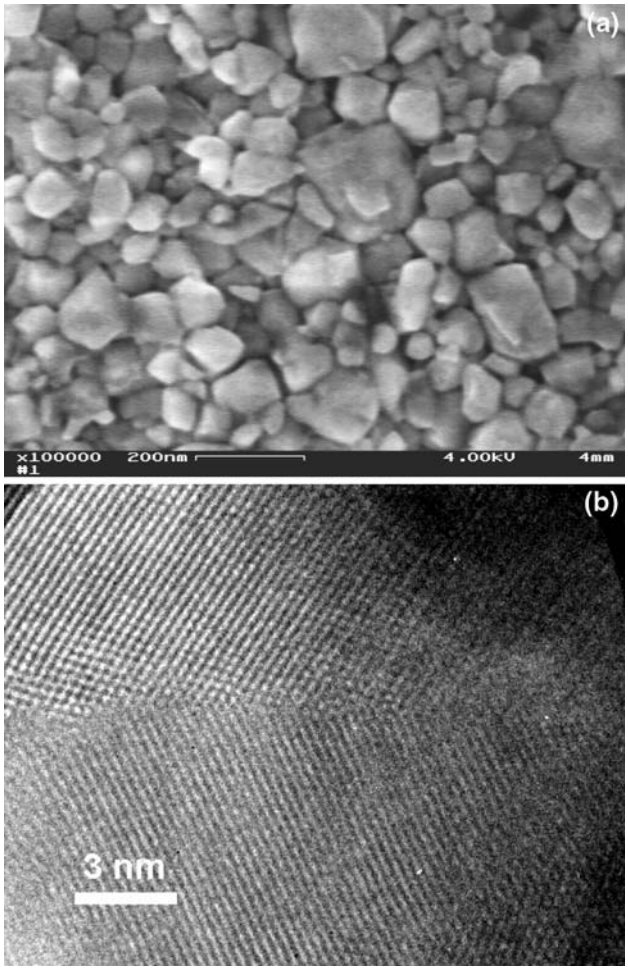

Fig. 1 (**a**) HRSEM image from polished surface of nc-MgO after hot-pressing at 790 °C for 4 h. (**b**) HRTEM image showing the disordered nature of the grain boundary region

Results

The processing parameters and the average grain size were summarized in Table 1. All the specimens exhibited nanometric grain size between 27 and 450 nm. The Archimedes densities ranged between 93.6 and 97.0% assuming a theoretical density of 3.58 g cm^{-3} (Table 1). However, HRSEM observations of these specimens revealed almost fully dense nanostructures (i.e., Fig. 1a); the observed volume fraction of the porosity was much lower than the measured porosity (3.0–6.4%). This difference may be associated with the excess free volume of the grain boundaries (gb's) in nanocrystalline materials [26]. Therefore, the density was calculated also by correcting for the excess free volume using Eq. 1 in [26] assuming a conservative grain boundary thickness of 1 nm; the corrected densities ranged between 96 and 97% of the theoretical density (Table 1). This indicates that the actual relative densities in these nanocrystalline specimens may be higher up to 3.4% of the measured values. Ultrafine

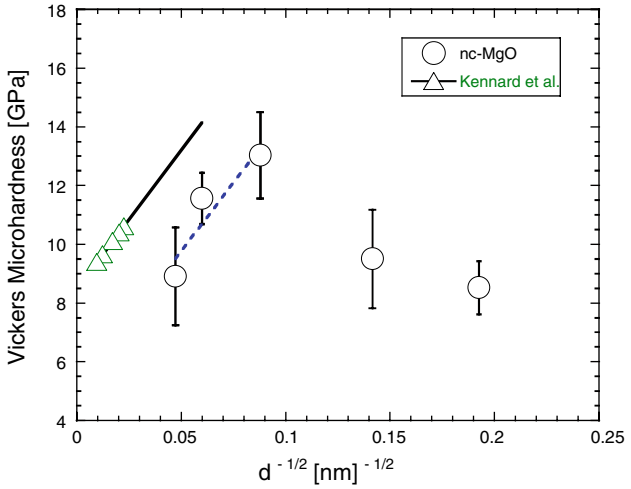

Fig. 2 Vickers microhardness versus the inverse of the square root of the grain size. The slope at larger grains (dashed line) is identical to the slope of the Kennard results (triangles) extrapolated to nanometer grain size range (solid line). See text for further details

mechanical polishing has revealed the morphology of the grain structure at the surface (Fig. 1a) which indicated on very weak strength of the gb's and consequent grain pull-outs. The gb's in HRTEM images were clearly visible (Fig. 1b); their width varied between 0.5 and 2.0 nm. The grain size distribution was fairly wide (Table 1) and revealed standard deviations as high as 60% of the average grain size. The microhardness results also showed relatively high standard deviations between 10 and 20% of the average values (Table 1). Nevertheless, the average microhardness values were clearly distinguishable from each other.

Plot of the microhardness versus inverse square root of the grain size (Fig. 2) showed increase in microhardness with decrease in the grain size down to 130 nm. This trend was reversed below 130 nm grain size, where microhardness was found to decrease. Such grain size dependence of the microhardness may follow that of the normal and the abnormal Hall–Petch behavior above and below 130 nm grain size, respectively, as shown below.

Discussion

The Hall–Petch behavior has been already observed in MgO alloy. Kennard et al. [27] measured the Knoop hardness of MgO lamellae in the directionally solidified MgO–$MgAl_2O_4$ eutectics with different lamellae thicknesses formed by controlled cooling rates. The hardness of the lamellar MgO versus the lamella spacing (2–10 μm range) followed the Hall–Petch behavior. The slope of the linear line fitted to our experimental data above 130 nm grain size (dashed line in Fig. 2) was identical to the slope of Auten et al. [23] results, extrapolated to the finer grain sizes (solid line in Fig. 2), hence confirming the Hall–Petch behavior in the present nc-MgO specimens.

In order to explain the abnormal Hall–Petch behavior in nc-MgO, the change in the microhardness is assumed to be directly related to the plasticity of the specimen. This assumption is justified since no microcracks were formed around the indents and at the indentations surfaces. The fracture energy due to microcracking during Vickers indentation of MgO (001) single crystals loaded in the range of 1 to 20 N was found to be 2.5% only of the total energy input, leading to elastoplastic behavior of MgO [28]. Therefore, the loading energy is put to plastic deformation and the strengthening effect should be associated with plastic deformation mechanisms.

With respect to the grain size effects, two main effects of the gb's should be considered. First, the gb acts as an obstacle to the dislocation motion by forming dislocation pile-ups; hence the corresponding Hall–Petch strengthening behavior with increase in the density of the gb's per unit volume. Second, assuming a finite thickness for the gb, the volume fraction of the gb's increases with the grain size decrease, especially in the nanometer size range. Since plasticity is a volumetric property, the overall microhardness values are affected both by plasticity of the grain interiors and the grain boundary 'phase.' Plasticity of the gb's, especially in ceramic systems, is expected to be far limited compared to that of the crystal. This is due to the disordered/amorphous nature of the gb's. Thus gb's at room temperature may accommodate some plastic deformation on the account of their free volume. However, due to absence of slip systems and non-active viscous flow at room temperature, any further deformation should be followed by bond breaking and nanocrack formation. Nevertheless, nanocracks can also act as dislocation sources as was observed in MgO [29]. Considering the grain boundary 'phase' as an amorphous, its hardness is a fraction of the hardness of its counterpart grain. The hardness of various fully dense amorphous metallic [30, 31] and ceramic [32, 33] compounds were found to be between 60 and 80% of the hardness of their corresponding crystalline form.

Eventually the pile-up strengthening effect ceases where it becomes energetically unstable below a critical grain size in the nanometer range [16]. Since the stress cannot be released further by dislocation slip, the grain boundary 'phase' should accommodate the corresponding strain. Therefore, at these nanometric grain sizes the plasticity may be controlled by the gb hardness, especially due to its high volume fraction.

Previous work has shown that the elastic modulus of the nanocrystalline MgO was lower by 13% compared to that of MgO with conventional grain size [34]. In order to

simplify the treatment we assume that the elastic modulus is independent of the grain size hence the elastic recovery at the indent during unloading is proportional to the load only. In addition, any effects of the time dependent plastic relaxations around the indent [35, 36] can be neglected due to the short duration of the present microhardness tests.

Using the composite model, the hardness of the isotropic polycrystalline material with high angle gb's may be described as the sum of the hardness contributed by the grain interiors and the gb's [18–20, 37, 38]. In such system, the volume of the gb's is determined by the grain boundary thickness (δ). The stressed volume beneath the indenter is subjected both to radial and compressive tensile stresses. Generally, one expects that the tangential tensile stresses will cause to formation of radial microcracks within the deformed volume in brittle materials. Nevertheless, it is well documented that radial microcracks during indentation of these ceramics form only above a critical load [39] and mainly near the free surfaces due to the lack of elastic constrain [40]. This indicates for low propensity of microcrack formation within the deformed volume, below this critical load. Physically, the absence of such radial microcracks within the deformed volume may be related to the relatively low magnitude of the tangential tensile stresses as is evidenced from their calculated distribution beneath the indenter in brittle systems [40].

Therefore, plastic deformation within the nc-MgO grains is expected to take place by dislocation glide due to the shear component of the compressive stresses. The dislocations formed in MgO under stress are known to be highly mobile even at room temperature and multiply by double-cross-slip mechanism. The hardness of the grain interior is related to the yield strength of the grain, which in turn is subjected to Hall–Petch strengthening. Thus, the hardness of the grain interior may be described by [41]:

$$H_g = H_0 + \frac{k}{\sqrt{d}}, \tag{1}$$

where, H_0 is the intrinsic hardness of the grain, k constant, and d is the grain diameter.

The constants H_0 and k can be estimated using the data from the literature. As was mentioned above following the Knoop hardness of MgO lamellae versus the lamella spacing (2–10 μm range), the Hall–Petch behavior with $k = 2.99$ GPa $\mu m^{1/2}$ was determined [27]. The value of H_0 is independent of the grain size and is fairly equal to microhardness of MgO single crystal averaged over its different crystallographic orientations. Averaging the microhardness over five different orientations (i.e., ⟨100⟩ and ⟨110⟩ on (001); ⟨001⟩, ⟨1$\bar{1}$1⟩, and ⟨1$\bar{1}$0⟩ on (110)) yields $H_0 = 6.5$ GPa [42]. This value is very close to those reported for MgO polycrystals, 6.3 [43] and 5.95 GPa [44, 45].

Following the composite model the effective hardness of nc-MgO is given by summation over the hardness of the grains and the gb's and follows that of the Hill's model: an algebraic average of the upper bound and lower bound of hardness [38]:

$$H_{effect}^{Hill} = \frac{(H_{effect}^{Reuss} + H_{effect}^{Voigt})}{2}, \tag{2}$$

where the effective upper bound (Voigt) and lower bound (Reuss) hardness were given by:

$$\frac{1}{H_{effect}^{Reuss}} = \frac{V_g}{H_g} + \frac{V_{gb}}{H_{gb}}, \tag{3a}$$

and

$$H_{effect}^{Voigt} = V_g \cdot H_g + V_{gb} \cdot H_{gb}, \tag{3b}$$

where V_g and V_{gb} are the volume fractions of the grain interior and the gb's, and H_g and H_{gb} are the hardness of the grain interior and the gb's, respectively.

The volume fraction of the grain interior and the gb's for a composite with Tetrakaidekahedron shape grains of caliper diameter d, and grain boundary thickness δ are given by [38, 46]:

$$V_g = \left(1 - \frac{3}{\sqrt{6}} \cdot \frac{\delta}{d}\right)^3 \tag{4}$$

and

$$V_{gb} = 1 - V_g. \tag{5}$$

Substituting V_g, V_{gb}, and H_g, respectively, from Eqs. 4, 5, and 1 into Eq. 3, and further into Eq. 2 yields the effective hardness of nc-MgO, subjected to grain size strengthening and weakening and its grain size dependence. The following values were used: $H_0 = 6.4$ GPa [42, 43], $k = 83.36$ GPa $nm^{1/2}$ [27], $H_{gb} = 0.7 \cdot H_0$ [30–33]. The

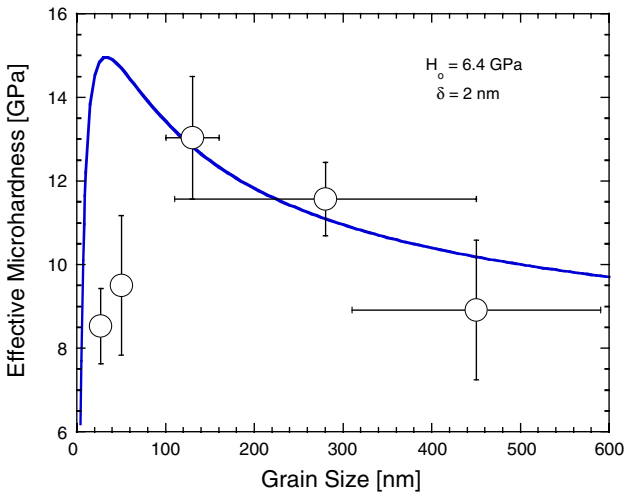

Fig. 3 Effective microhardness of nc-MgO versus the grain size (open circles) and its fit to the composite model (solid line)

better fit was found with grain boundary thickness $\delta = 2$ nm. The calculated curve is shown in Fig. 3 together with the experimental microhardness values. The standard deviations of the microhardness as well as of the average grain size were also indicated. The good-fit of the experimental values to the calculated curve indicates that composite model may be applied successfully for describing both normal and abnormal Hall–Petch behavior during plastic deformation of ductile nc-MgO. The lower experimental data at the smallest grain sizes may be due to extensive nanocracking at the gb's.

Summary and conclusions

Fabrication of dense nc-MgO by hot-pressing enabled to measure the microhardness versus the average grain size. The microhardness followed the Hall–Petch behavior with decreasing the grain size down to 130 nm. However, abnormal behavior of microhardness was observed below this grain size. The experimental data were analyzed using a composite model that considers dislocation hardening of the grains and plastic flow under compression within the gb's. The good agreement between the experimental and the calculated values indicates that gb's may have significant effect on strengthening and ductility of nc-MgO ceramics in the nanometer size range. Critical grain size exists below which limited plastic deformation within the grains and nanocracking at gb's enhances the brittleness of the ceramic.

Acknowledgement The support of the Israel Ministry of Science through the grant no. 1090-1-00 is gratefully acknowledged.

References

1. Morgan PED, Scala E (1965) In: Kuczynski GC, Hooton NA, Gibbon CF (eds) Sintering and related phenomena. Breach Sci Pub, NY
2. Pampush R (1979) Ceramurgia Int 5:76
3. Itatani K, Nomura M, Kishioka A, Kinoshita M (1986) J Mater Sci 21:1429. doi:10.1007/BF00553284
4. Itatani K, Yasuda R, Howell FS, Kishioka A (1997) J Mater Sci 32:2977. doi:10.1023/A:1018649222749
5. Vieira JM, Brook RJ (1984) J Am Ceram Soc 67:450
6. Pampush R, Tomaszewski H, Haberko K (1975) Ceramurgia Int 1:81
7. Wilshire B (1995) Br Ceram Trans 94:57
8. Ehre D, Gutmanas EY, Chaim R (2005) J Eur Ceram Soc 25:3579
9. Chaim R, Shen Z, Nygren M (2004) J Mater Res 19:2527
10. Rice RW, Wu CC, Borchelt F (1994) J Am Ceram Soc 77:2539
11. Majumdar BS, Burns SJ (1987) J Mater Sci 22:1157. doi:10.1007/BF01233104
12. Chokshi AH, Rosen A, Karch J, Gleiter H (1989) Scripta Metall 23:1679
13. Jang JSC, Koch CC (1990) Scripta Metall Mater 24:1599
14. Lu K, Wei WD, Wang JT (1990) Scripta Metall Mater 24:2319
15. Gerstman VY, Hoffmann M, Gleiter H, Birringer R (1994) Acta Mater 42:3539
16. Nieh TG, Wadsworth J (1991) Scripta Metall Mater 25:955
17. Lian J, Baudelet B (1993) Nanostruct Mater 2:415
18. Wang N, Wang Z, Aust KT, Erb U (1995) Acta Metall Mater 43:519
19. Masumura RA, Hazzeldine PM, Pande CS (1998) Acta Mater 46:4527
20. Song HW, Guo SR, Hu ZQ (1999) Nanostruct Mater 11:203
21. Zaichenko SG, Glezer AM (1999) Interface Sci 7:57
22. Singh RN, Coble RL (1974) J Appl Phys 45:981
23. Auten TA, Radcliffe SV, Gordon RB (1976) J Am Ceram Soc 59:40
24. Bahr DF, Kramer DE, Gerberich WW (1998) Acta Mater 46:3605
25. Gaillard Y, Tromas C, Woirgard J (2004) Acta Mater 54:1409
26. Chattopadhyay PP, Pabi SK, Manna I (2001) Mater Chem Phys 68:80
27. Kennard FL, Bradt RC, Stubican VS (1976) J Am Ceram Soc 59:160
28. Loubet JL, Georges JM, Marcheshini O, Meille G (1984) J Tribol 106:43
29. Higashida K, Narita N, Onodera R, Minato S, Okazaki S (1997) Mater Sci Eng A 237:72
30. Wolff U, Pryds N, Johnson E, Wert JA (2004) Acta Mater 52:1989
31. Baricco M, Castellero A, Di Chio M et al (2007) J Alloys Compd 434–435:183
32. Wang HL, Lin CH, Hon MH (1997) Thin Solid Films 310:260
33. Li Q, Yu YH, Bhatia CS, Marks LD et al (2000) J Vac Sci Technol A 18:2333
34. Yeheskel O, Chaim R, Shen Z, Nygren M (2005) J Mater Res 20:719
35. Hammond BL, Armstrong RW (1988) Phil Mag Lett 57:41
36. Sangwal K, Gorostiza P, Servat J, Sanz F (1999) J Mater Res 14:3973
37. Bush MB (1993) Mater Sci Eng A 161:127
38. Chaim R (1997) J Mater Res 12:1828
39. Cook RF, Pharr GM (1990) J Am Ceram Soc 73:787
40. Larsson PL, Giannakopoulos AE (1998) Mater Sci Eng A 254:268
41. McColm IJ (1990) Ceramic hardness. Plenum, New York
42. Roberts SG (1988) Phil Mag A 58:347
43. Cook RF, Liniger EG (1992) J Mater Sci 27:4751. doi:10.1007/BF01166017
44. Rice RW (1971) In: Kriegel WW, Palmour H III (eds) Materials science research. Plenum Press, NY
45. Zhang J, Sakai M (2004) Mater Sci Eng A 381:62
46. Wang N, Palumbo G, Wang Z, Erb U, Aust KT (1993) Scripta Metall Mater 28:253